Ultrafast Solar-Blind Ultraviolet Detection by Inorganic Perovskite $CsPbX_3$ Quantum Dots Radial Junction Architecture

Jiawen Lu, Xuexi Sheng, Guoqing Tong, Zhongwei Yu, Xiaolin Sun, Linwei Yu, Xiangxing Xu,* Junzhuan Wang, Jun Xu, Yi Shi, and Kunji Chen*

Inorganic $CsPbX_3$ (X = Cl, Br, I, or hybrid among them) perovskite quantum dots (IPQDs) are promising building blocks for exploring high performance optoelectronic applications. In this work, the authors report a new hybrid structure that marries $CsPbX_3$ IPQDs to silicon nanowires (SiNWs) radial junction structures to achieve ultrafast and highly sensitive ultraviolet (UV) detection in solar-blind spectrum. A compact and uniform deployment of $CsPbX_3$ IPQDs upon the sidewall of low-reflective 3D radial junctions enables a strong light field excitation and efficient down-conversion of the ultraviolet incidences, which are directly tailored into emission bands optimized for a rapid photodetection in surrounding ultrathin radial p-i-n junctions. A fast solar-blind UV detection has been demonstrated in this hybrid IPQD-NW detectors, with rise/fall response time scales of 0.48/1.03 ms and a high responsivity of 54 mA W^{-1}@200 nm (or 32 mA W^{-1}@270 nm), without the need of any external power supply. These results pave the way toward large area manufacturing of high performance Si-based perovskite UV detectors in a scalable and low-cost procedure.

Inorganic perovskite quantum dots (IPQDs) of cesium–lead–halide, dubbed as $CsPbX_3$ where X stands for the elements of Cl, Br, I, or a mixture of them,[1] are promising optoelectronic materials for photovoltaics, display, and photodetection.[2–5] By means of compositional and size control, the optical bandgaps of the $CsPbX_3$ QDs can be easily controlled for specific wavelength light emission or absorption.[1,2] More importantly, the air-exposure stability of the IPQDs is superior compared to their organic counterparts,[3] thanks to the replacement of organic methyl ammonium with inorganic Cs cations.[4–7] For example, the mostly studied organic–inorganic hybrid perovskite of methyl ammonium lead triiodide ($MAPbI_3$) is highly sensitive to moisture in air, while the inorganic perovskite such as $CsPbBr_3$ QDs can survive a lasting exposure to humid air of 90%–95% RH for 15 d without significant change in XRD patterns or color.[6] This is critical for practical photoelectronic applications, where long-term stability and cost-effectiveness are crucial. Meanwhile, the high quantum efficiency and wavelength tunability of IPQDs are advantageous for achieving sensitive photodetections. Particularly, solar-blind ultraviolet (UV) detection to wavelengths <300 nm has been the key technology in flame detection, remote security monitoring, and missile approaching warning system.[8–10] So far, solar-blind UV detectors are usually manufactured from expensive III-V crystals upon small-sized and expensive substrates. If the UV detectors can be fabricated over large area, a higher spatial resolution in solar-blind detection or even direct imaging can be achieved.[11] To this end, a low-cost and scalable UV detector manufacturing has to be established, ideally based on the mature Si thin film technology. Recently, Si-based solar-blind UV detection has been demonstrated by using c-Si PN junction diodes, with the aid of rare-earth-element assisted down conversion in a shadowed-sidewall-incident configuration.[12] However, the optical absorption cross-section of rare-earth-elements is relatively small due to the f–f transition nature,[13] while the planar diode junction and the sidewall-incident structure[12] are also inefficient for achieving an efficient solar blind UV detection.

Recently, various materials have been explored, including Si QDs, rare-earth-elements and polymers[14–19] in order to convert ultraviolet incidences into longer wavelengths suitable for Si-based light absorption and sensing.[20–22] Unfortunately, the efficiency remains low either due to a low internal quantum efficiency in the light down-converting elements (for example, in Si QDs[23]) or/and to an inefficient light management configuration that degrades largely the performance of light conversion and detection.[14–19] To this end, the high quantum yields of IPQDs are very promising to achieve a highly efficient down-conversion. If the outstanding optoelectronic properties of the IPQDs can be married to an advantageous 3D radial p-i-n (PIN)

J. Lu, G. Tong, Z. Yu, X. Sun, Prof. L. Yu, Prof. J. Wang, Prof. J. Xu, Prof. Y. Shi, Prof. K. Chen
National Laboratory of Solid State Microstructures
School of Electronics Science and Engineering
Collaborative Innovation Center
of Advanced Microstructures
Nanjing University
Nanjing 210093, P. R. China
E-mail: yulinwei@nju.edu.cn

X. Sheng, Prof. X. Xu
Jiangsu Key Laboratory of Biofunctional Materials
School of Chemistry and Materials Science
Nanjing Normal University
Nanjing 210046, P. R. China
E-mail: xuxx@njnu.edu.cn

DOI: 10.1002/adma.201700400

junction architecture, a highly efficient, ultrafast and sensitive UV detection can be expected.

In this work, we propose a new hybrid 3D architecture that integrates high quantum yield IPQDs upon hydrogenated amorphous silicon (a-Si:H) radial junctions (RJ) constructed over silicon nanowire (SiNW) structure, and demonstrate an ultrafast and efficient optoelectronic down-conversion for solar blind UV detection. The IPQD layers are uniformly coated upon the sidewalls of the RJs, and thus enjoy a strong light field excitation and absorption. Then, the down-converted photon signals are completely trapped and rapidly detected by the surrounding 3D RJ structures, where a very thin intrinsic a-Si:H absorb layer (<80 nm) is used to boost a fast photocarrier separation and response. All these factors combined lead to an ultrafast and sensitive solar blind UV detection without the need of external power supply, with rise/fall times of only 0.48 ms/1.03 ms and responsivity of 54 mA W^{-1}@200 nm (or 32 mA W^{-1}@270 nm), manufactured via a room temperature, low-cost, and readily scalable thin film deposition and solution process.

Controlled arrested precipitation of Cs^+, Pb^{2+}, and X^- ions into $CsPbX_3$ nanoparticles is obtained by reacting Cs–oleate with a Pb(II)–halide in a high boiling solvent (octadecene) at about 150 °C.[24] In order to dissolve PbX_2 and to colloidally stabilize the nanoparticles, a 1:1 mixture of oleylamine and oleic acid was added into octadecene. Owing to the coordination nature of the chemical bonding in these compounds, the nucleation and growth kinetics are very fast (for example, in several seconds).[25] By combining appropriate ratios of PbX_2 salts, $CsPb(Cl/Br)_3$ and $CsPb(Br/I)_3$ can be readily produced.[25,26] The $CsPbX_3$ QDs show bright colors under daylight and UV radiation and the quantum yields of which can be up to 90%.[24]

The thin film solar cells composed of SiNW radial junctions were fabricated via a tin (Sn) nanoparticle catalyzed vapor–liquid–solid (VLS) growth mechanism on AZO-coated (AZO: aluminum-doped zinic oxide) glass in a plasma enhanced chemical vapor deposition (PECVD) system, with a final multilayer structure comprising p-doped SiNWs in the core, radially coated layers of intrinsic a-Si:H absorber, n-doped a-Si:H emitter, and top ITO contact, as illustrated schematically in **Figure 1**b. Scanning electron microscopy (SEM) images of the SiNW RJs are provided in **Figure 2**b. More experimental details are provided in our previous works.[20–22,27–29]

The colloidal $CsPbX_3$ QDs are spin-coated over the SiNW radial junctions (RJs), in a procedure as depicted schematically in , Figure 2a. According to the SEM characterizations of the RJs with or without QDs coatings, as shown in Figure 2b,c respectively, quite a conformal coating of the $CsPbX_3$ QDs film has been achieved over the whole RJs surface, despite a rough and complex surface. A close SEM examination of the IPQDs-loaded RJ sidewalls (Figure 2d) reveals a shallow but regular square-motif, which can be assigned to a compact packing of $CsPbX_3$ QDs, while a similar pattern is also observed in separate transmission electron microscopy (TEM) characterization of the same QDs thin film deposited on flat substrate as found in Figure 2e. These observations indicate that a complete, compact, and uniform IPQDs thin film has been deployed successfully over the SiNW RJ framework. This has been the key to integrate the IPQDs into a 3D photonic architecture without smearing their geometric feature that is important for strong light trapping effect.

As witnessed in Figure 1c, the IPQDs have a strong absorption to the high energy UV photons with a sharp decrease at around 300 nm. The PL emission from the IPQDs in Figure 1c locates

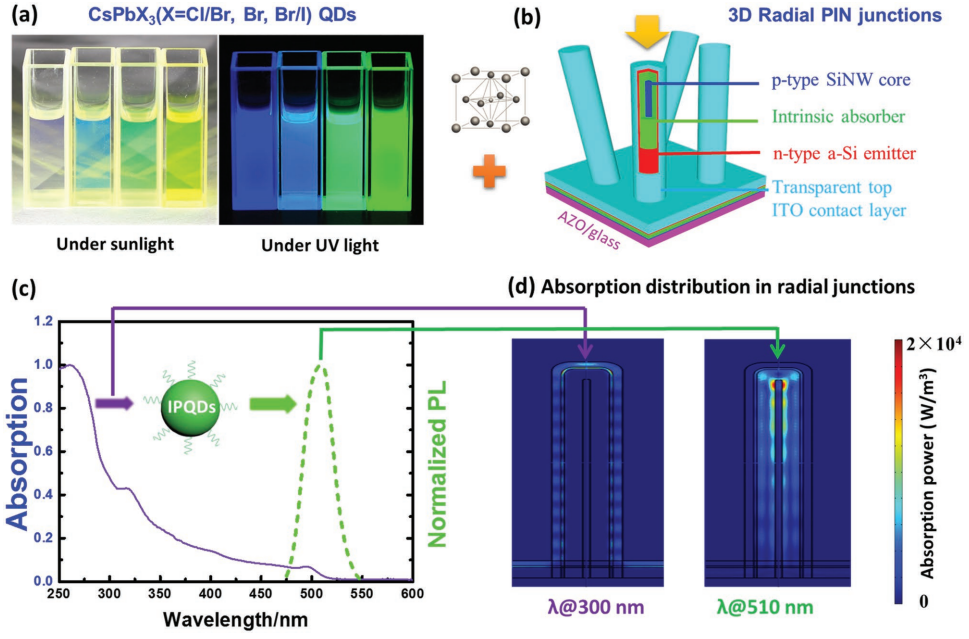

Figure 1. a) Photos of the inorganic $CsPbX_3$ QDs solution in cyclohexane under daylight or UV light illuminations; b) a schematic illustration of the multilayer a-Si thin film PIN radial junction structure constructed upon SiNWs; c) the absorption and normalized photoluminescence (PL) spectra of typical $CsPbBr_3$ QDs, with the corresponding simulated absorption power distribution profile, located at 300 and 500 nm (for the absorption and emission peaks) wavelengths, displayed in d).

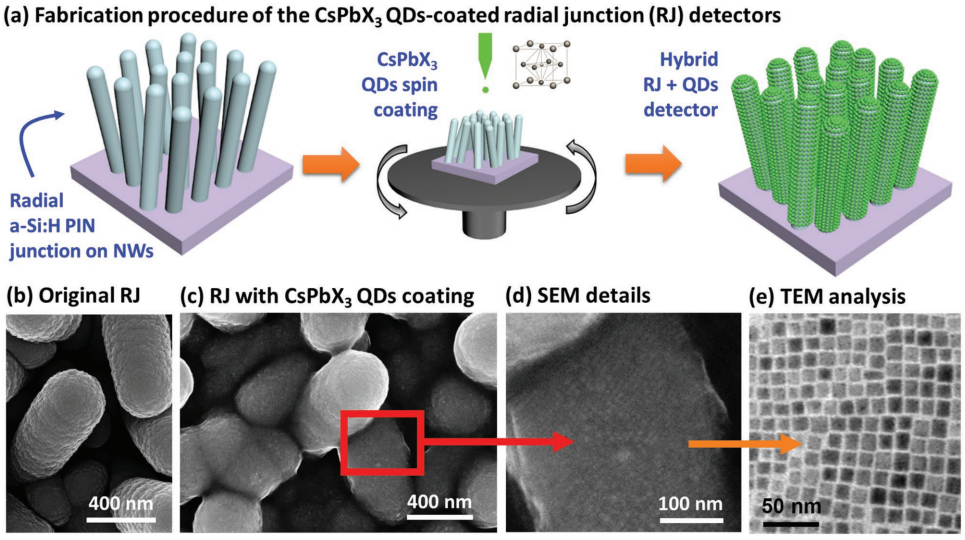

Figure 2. a) Illustration of the spin-coating of $CsPbX_3$ QDs thin film over 3D SiNW-RJ architecture, with corresponding SEM images of the RJ units, b) before and c) after QDs coating. The enlarged SEM view of the QDs coated RJ sidewall. d) A similar square motif of $CsPbX_3$ QDs to that observed in TEM characterization e).

at a longer wavelength of 510 nm, which is indeed tunable by changing the halide element composition as will be discussed later. It is important to note that, without the IPQDs-coating, the UV photon incidence (<320 nm) will be completely absorbed and screened off by the outer ITO and n-type doped a-Si:H window layer, as witnessed in the light absorption distribution simulation in the left panel in Figure 1d (see refs. [30,31] for more simulation details in our previous works). As a consequence, there is little chance for the incident UV signals to arrive and get absorbed by the inner i-layer in the radial PIN junction, that is no the RJ units by themselves with top ITO contact and doped a-Si:H demonstrate no response to solar blind wavelengths <300 nm, as witnessed in the external quantum efficiency (EQE) response of a-Si:H RJ units in **Figure 3**a. In contrast, with a compact sidewall-coating of IPQD layer, the incident of UV signals are first absorbed by the outer IPQDs, and then down-converted into longer wavelengths at ≈510 nm, which according to the EQE response spectrum in Figure 3a, is the highest response region of a-Si:H RJs. This dramatic difference can also be learnt from the simulated light absorption distribution under 510 nm

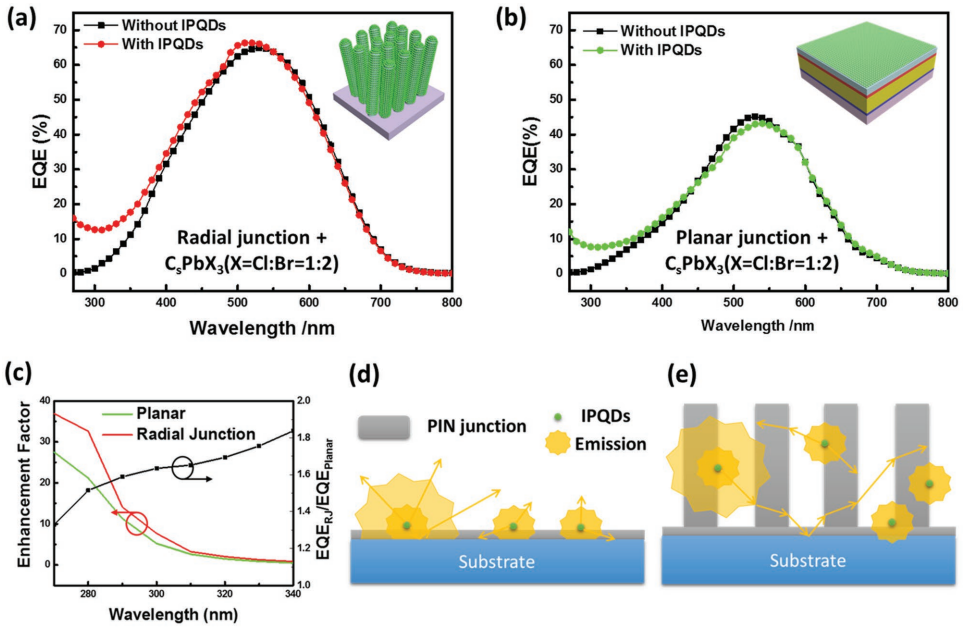

Figure 3. a,b) The EQE responses of radial junction (RJ) and planar junction detectors, with and without IPQDs decoration, respectively; c) the wavelength-dependent EQE enhancement of the RJ and the planar junctions; d,e) the different light harnessing performances of the reemitted and down-converted photons from IPQDs among the RJ and the planar structures.

incidence in Figure 1d,[30,31] where the light field can propagate into the RJ structure and be absorbed/detected by the photoactive i-layer in the radial PIN junctions.

To testify the UV detection capability of this unique IPQDs-loaded RJ detector, we fabricated photodetectors in both radial and planar junction thin film diode architectures, all with the same $CsPbX_3$ (X = Cl/Br = 1:2) IPQDs coating procedure. As seen in Figure 3a,b, the EQE characterizations are carried out over a full spectrum from solar blind UV wavelengths (280 nm) to 800 nm that covers the whole absorption range of hydrogenated a-Si:H (350–750 nm). Compare to their planar counterpart (in Figure 3b), the IPQDs and RJ units demonstrate a 50% stronger light absorption and response, owing to a strong light trapping effect that minimizes the reflection losses. Note that, Figure 3a,b indicates that, without the IPQDs coating, none of the RJ and planar units can detect UV signals <300 nm, while clear UV responses (from 350 nm to deep UV 270 nm) are installed for both the planar and RJ detectors when IPQD layers are spin-coated. Interestingly, from 310 nm to even shorter wavelength, the EQE response seems to rise steadily into the solar blind region, but this trend cannot be followed as limited by the spectrum range of our EQE characterization system. In order to gauge the contributions from the IPQDs-assisted down-conversion, an enhancement factor is defined for both the RJ and planar detectors as

$$E_{dc} \equiv \frac{EQE_{with\ QDs} - EQE_{without\ QDs}}{EQE_{without\ QDs}} \quad (1)$$

According to the plots in Figure 3c, the IPQDs-coated RJ detectors can easily achieve a 38 (or 26) times stronger EQE response @270 nm in RJ (or planar) PIN junction structure, providing an important basis for achieving a sensitive Si-based UV detection.

Furthermore, a higher UV response performance of the IPQDs-loaded RJ detectors, over the planar ones, can be assigned to the strongly enhanced light trapping and absorption achieved in the 3D RJ framework.[32,33] This can be explained with the aid of the schematic diagrams in Figure 3d,e, where the harnessing of down-converted photons, reemitted by the IPQDs, are far more efficient in a 3D SiNW radial junction structure compared to that in a planar junction architecture. More specifically, if the IPQDs are spread over planar surface, their reemissions could easily escape from the top and open interface, while this portion of loss is largely suppressed due to a strong light confinement within the RJs framework (as depicted in Figure 3e), leading to a more efficient UV response.

The impact of the bandgap engineering of $CsPbX_3$ IPQDs on the UV responses is also investigated. In principle, the PL emission from the IPQDs is tuned and targeted at the maximal EQE response of the RJs (≈500 nm), by varying the halide ratio in $CsPbX_3$ IPQDs. Four different $CsPbX_3$ IPQDs are prepared and marked as a–d in **Figure 4**e, with gradually decreasing optical bandgaps, as inferred from their shifting absorption edge and PL emission bands. When the Br^- and Cl^- ion ratio is 1:1 (in type-a IPQDs), the PL emission peak locates at around 450 nm, deviated to short wavelength from the maximal EQE response of RJs. This leads to only a tiny increase in the UV response, because the reemitted short wavelengths, by themselves, locate at the falling edge of the EQE spectrum of a-Si:H RJs. When the amount of Br^- ions is increased (in type-b IPQDs), their PL emission band is red-shifted to ≈480 nm, the UV EQE response in the solar blind range has been strongly boosted to 22% @270 nm, while an even higher EQE response is expected into deeper solar blind wavelengths. However, when the Cl^- ions are completely substituted by Br^- ions (in type-c IPQDs) or with I^- ions (in type-d), the EQE responses in the UV range does not increase further, despite their PL emission bands in 510 and 540 nm, respectively. This could indicate that, the PL emissions at around 500 nm fall already in the optimal EQE plateau-range, and thus other factors like the absorption and thickness fluctuations could become dominant. Nevertheless, these results highlight the important potential of bandgap engineering capability of IPQDs in fine-tuning the UV detection performance in the hybrid IPQDs-loaded RJ units

The UV detection speeds of the IPQDs-RJ detectors are evaluated under varied laser signals and shown in **Figure 5**, where laser beams @280 nm are modulated at different frequencies

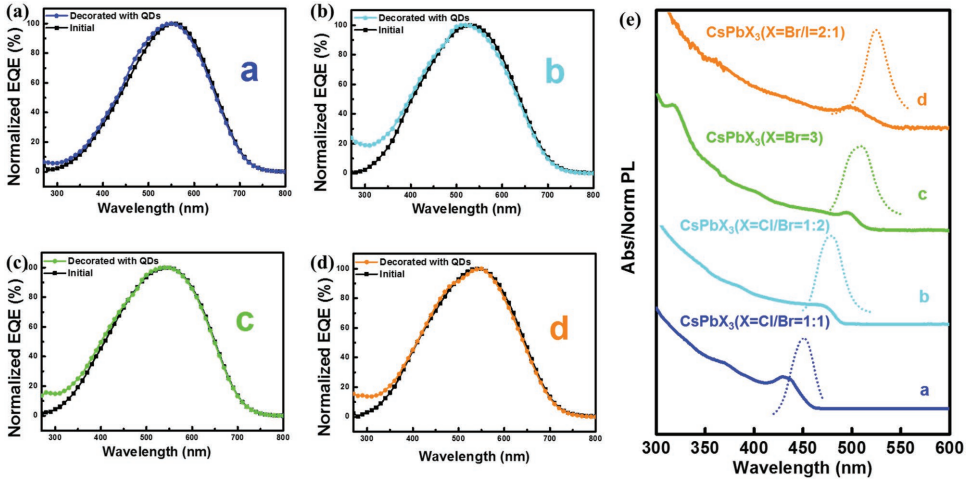

Figure 4. a–d) The normalized EQE responses of type (a–d) RJ samples with or without inorganic perovskite QDs coating. e) The evolution of the absorption edges and the PL emission bands of the corresponding IPQDs with different halide compositions.

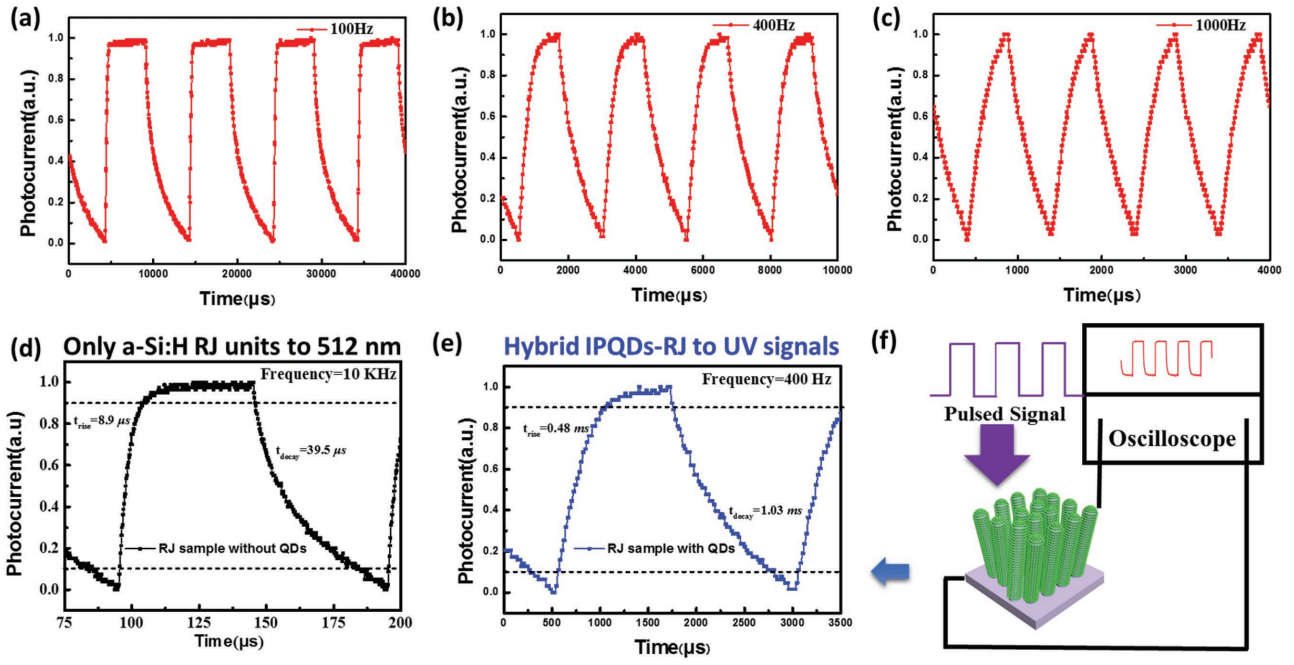

Figure 5. Time response characteristics of the device under different pulsed light illumination a) 100 Hz, b) 400 Hz, and c) 1000 Hz. d) Time response characteristics of the device without QDs @10 kHz. e) The magnified and normalized plots of one response cycle in b). f) Schematic illustration of photoresponse speed of the device.

ranging from 10 Hz to 10 kHz and photocurrent signals are recorded by oscilloscope in real time. As we can see, the IPQDs-RJ detector can catch up the alternating stimulations up to ≈1 kHz. According to the photocurrent response profile recorded @ f = 400 Hz and shown in Figure 5e, the rise (t_{rise}) and the fall (t_{decay}) time scales are extracted (according to ref. [34]) to be 0.48 and 1.03 ms, respectively. It is important to note that, the a-Si:H RJ (with a very thin intrinsic i-layer of only 80 nm) along can response to the visible 512 nm wavelength modulation far more rapidly with rise/fall time scales of only 8.9 and 39.5 μs, as witnessed in Figure 5d. This thus excludes the a-Si:H RJs as the rate-limiting factor in the response speed. Meanwhile, the UV light down-conversion by the IPQDs is also known to be a fast process (typically in nanoseconds).[24,25] So, it is possible that the electric coupling between the IPQDs coating layer and the beneath ITO layer could be the reason that limits further increase of the UV response speed, which will be investigated in our future work.

Further on, in order to implement the IPQDs-RJ units for selective solar-blind UV detection, a subtractive device configuration has been adopted, as schematically illustrated in **Figure 6**a, where a pair of two a-Si:H RJ units with the same dimension and density are prepared in the same batch of PECVD growth. Then, only one of them is coated with colloidal $CsPbX_3$ QDs (X = Cl/Br = 1:2), while the other one without IPQDs serves as the background reference. By subtracting the EQE response of the IPQDs-loaded RJ units with that of the IPQDs-free reference, we calculate the spectral responsivity (R) of the device with the following formula

$$R = \frac{I_{\text{with QD}} - I_{\text{without QD}}}{I_{\text{Si-light}} - I_{\text{Si-dark}}} R_{\text{Si}} \quad (2)$$

where R_{Si} is the spectral responsivity of standard Si photodetector, which is already known and thus provides a reference to determine and calibrate the actual power density incidence at different wavelengths. $I_{\text{Si-light}}$ and $I_{\text{Si-dark}}$ are the photocurrents measured by the standard Si photodetector at different wavelength with or without light signals. Figure 6b shows the photocurrent of both IPQDs-loaded or IPQDs-free samples. Obviously, the photocurrents from the IPQDs-loaded RJs are two orders of magnitude stronger than that of IPQDs-free reference for the deep UV incident wavelengths at 200 nm. The photocurrent difference response between the IPQDs-RJ sample and the reference RJ samples are extracted and presented in Figure 6c, where a peak responsivity of 54 mA W^{-1}@200 nm (or 32 mA W^{-1}@270 nm) into the solar blind spectrum has been achieved with this subtractive IPQDs-RJ UV detector.

In addition, the air-exposure stability of the IPQD-RJ detector is also testified. As witnessed in Figure S1 in the Supporting Information, the hybrid IPQD-RJ detectors can retain 70% peak responsivity after air exposure for 30 d at around 25 °C without particular encapsulation, which is indeed an important advantage of the inorganic perovskite QDs detectors, compared to their organic–inorganic counterparts $MAPbI_3$ that is highly sensitive to the moisture in air.

Compared to the Si-based or perovskite and QDs-based hybrid UV photodetectors in the literature, as summarized in **Table 1**,[3,12,26,35–42] our IPQDs-RJ detector has achieved an outstanding response speed without the need of any external power supply. Note that, most commercial ultraviolet photodiodes are built on expensive and high quality epitaxial films of gallium nitride. Otherwise, the UV detection can be realized by adopting zinc oxide,[40] silicon carbide,[11] or gallium phosphide,[43] but relies on high external bias voltage.[35]

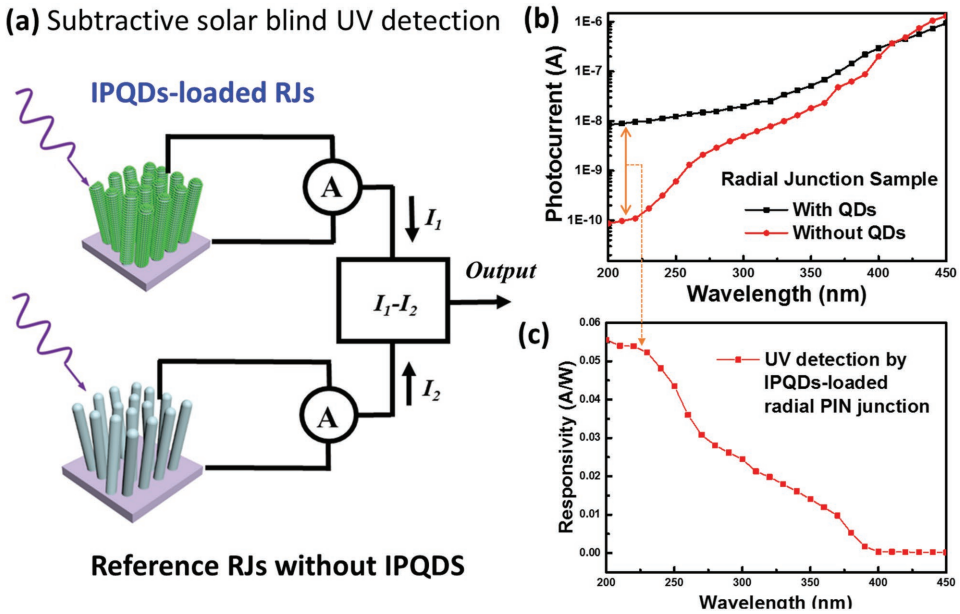

Figure 6. a) A subtractive UV detection setup based on the IPQDs-loaded radial junction (RJ) units. b) Photocurrents of the RJ units with or without IPQDs coating. c) The extracted net photocurrent responsivity to solar blind UV wavelengths.

Nevertheless, the response speeds are still low compared to what has been achieved in this work, as detailed in Table 1. In addition, among the self-powered UV detectors, a self-powered high peak responsivity of 54 mA W^{-1}@200 nm has been achieved in the IPQDs-RJ detector, which is the record among all the perovskite or polymer-based UV detectors reported in the literature.[12,26,39] More importantly, this Si-based IPQDs-decorated RJ detector can be manufactured via a low-cost and readily scalable thin film technology upon cheap glass or even flexible substrates.

In conclusion, a high performance solar blind UV detection has been achieved in a novel 3D hybrid $CsPbX_3$ IPQDs and RJ

Table 1. Comparison of this work to the perovskite or QD-based UV detectors in the literature.

Materials and structure	Spectral window [nm]	Response time t_{rise}/t_{decay}	Responsivity (self-powered)	Responsivity (under bias)	Reference
$CsPbX_3$ QDs/a-Si radial PIN junction/glass	200–400	0.48 ms/1.03 ms	54 mA W^{-1} @200 nm 32 mA W^{-1} @270 nm	–	This work
ITO/$MAPbCl_3$/glass	340–400	–/≈1 ms	–	18 A W^{-1} @385 nm V_{bias} = 5 V	[8]
Au/ZnO nanoparticle film/glass	370–400	<0.1 s/≈0.1 s	–	61 A W^{-1} @370 nm V_{bias} = 120 V	[38]
Ag/Al nanoparticles/ZnO nanorods/SiO_2	300–400	0.8 s/0.85 s	–	1.59 A W^{-1} @325 nm V_{bias} = 5 V	[43]
EuHD doped PMMA/Au/Si pn diode	280–450	≈1 s/≈1 s	–	–	[17]
$CsPbI_3$ NCs/Au/SiO_2/P^+ Si	400–500	24 ms/29 ms	≈20 mA W^{-1} @405 nm	–	[29]
a-Si/a-SiC/AZO/glass	320–500	–	≈100 mA W^{-1} @320 nm	–	[39]
Al/SiNCs/PEDOT:PSS/ITO/glass	270–400	–	20 mA W^{-1} @310 nm	–	[42]

structure. The high quantum yield of $CsPbX_3$ QDs with tunable bandgap over the entire visible spectral region has been integrated into photonic a-Si:H RJ, where strong light trapping, absorption, and excitation effects combined lead to an ultrafast UV wavelength detection with rise/fall times scales of on 0.48/1.03 ms and a peak responsivity of 54 mA W^{-1} at 200 nm, without the need of any external power supply. These results pave the way toward large area manufacturing of high performance Si-based perovskite UV detectors in a scalable and low-cost procedure.

Experimental Section

Materials: PbI_2 (AR. 98%), $PbBr_2$ (AR. 99%), $PbCl_2$ (AR. 99%), $ZnCl_2$ (AR. 99.95%), Cs_2CO_3 (99.9%), cyclohexane (99.9%), and oleylamine (90%) were purchased from Aldrich and used as received without further purification. The oleic acid (90%) and 1-octadecene (ODE, 90%) were purchased from Alfa Aesar.

Synthesis of $CsPbX_3$ (X = Cl, Br, I, or Mixture) QDs: All the synthesis was carried out in a Schlenk line with a vacuum pump and protected by Ar. Typically, ODE (5 mL), oleylamine (0.5 mL), oleic acid (0.5 mL, OA), and PbX_2 (0.188 mmol, e.g., $PbBr_2$ 69 mg or Cl/Br, Br/I mixtures) were loaded into 50 mL three-neck flask and treated under vacuum for 1 h at 120 °C. After complete dissolution of the PbX_2 salt, the temperature was raised to 150 °C and the Cs–oleate solution (0.4 mL) was quickly injected and let react for 5 s. The Cs–oleate solution was prepared by dissolving 2.5 mmol Cs_2CO_3 in 40 mL ODE with 2.5 mL OA heating at 130 °C for 30 min. The reaction mixture was cooled by an ice-water bath. The $CsPbX_3$ QDs were separated by direct centrifugation of the reaction solution at 12 000 rpm for 10 min. The supernatant was discarded with the small amount of liquid residual in the centrifugation tube carefully adsorbed by a paper tip. The precipitated $CsPbX_3$ QDs were redispersed in cyclohexane forming a long-term stable colloidal solution. The quantum yield of the as prepared $CsPbX_3$ QDs in cyclohexane is 40%–70%, measured by using standard fluorescence dyes as reference.[2]

Radial PIN Junction Fabrication: A 2 nm Sn layer was first evaporated on AZO glass substrate. The substrate was loaded into a PECVD system, where a hydrogen plasma treatment was applied at 200 °C to transform the Sn layer into discrete Sn droplets. Then, the substrate temperature was raised to 400 °C with the introduction of a mixture of silane and dopant (B_2H_6) gases to grow p-type SiNWs, via a VLS mode, to a length of around 1 µm with a mean diameter of 30–40 nm in the middle. After that, the intrinsic a-Si:H absorber and n-type doped a-Si:H emitter were deposited upon the SiNW cores at 150 °C. Finally, the top transparent ITO electrodes were deposited through shadow masks by magnetron sputtering.

IPQDs Radial Junction Detector Fabrication: The $CsPbX_3$/cyclohexane solution (0.1 mL) was spin-coated onto the radial junction structure via a two-step procedure (first 400 rpm for 10 s and then 1000 rpm for 50 s). The active region of the hybrid QDs radial junction UV detector unit measures 3 mm by 1 mm with a density of about 5×10^8 cm^{-2}. Thus there are roughly tens of millions of IPQD-loaded radial junctions that contribute in parallel to the photoresponse and detection. The photocurrent signals were extracted from the top ITO and the bottom AZO electrodes.

Response Speed Characterization: Monochromatic (λ = 280 nm) illumination was provided by using a pulsed laser. The light source was modulated at different frequencies ranging from 10 Hz to 10 kHz. The response was measured using a Tektronix TDS2012B oscilloscope.

Supporting Information

Supporting Information is available from the Wiley Online Library or from the author.

Acknowledgements

J.L. and X.S. contributed equally to this work. The authors acknowledge the financial supports from the National Natural Science Foundation of China under Nos. 61674075, 11274155 and 51572120, the National Basic Research 973 Program under Grant Nos. 2014CB921101, 2013CB632101, and 2013CB932900, the Jiangsu Excellent Young Scholar Program under No. BK20160020, the Scientific and Technological Support Program in Jiangsu province under No. BE2014147-2, Jiangsu Shuangchuang Program, the Fundamental Research Funds for Central Universities, and the support from the Key Laboratory of Advanced Photonic and Electronic Materials.

Note: The first name of Prof. Xiangxing Xu was corrected in the article byline on June 13, 2017, after initial publication online.

Received: January 20, 2017
Revised: February 16, 2017
Published online: March 29, 2017

[1] J. S. Steckel, J. Ho, C. Hamilton, J. Xi, C. Breen, W. Liu, P. Allen, S. Coe-Sullivan, *J. Soc. Inf. Disp.* **2015**, *23*, 294.
[2] X. Li, Y. Wu, S. Zhang, B. Cai, Y. Gu, J. Song, H. Zeng, *Adv. Funct. Mater.* **2016**, *26*, 2435.
[3] V. Adinolfi, O. Ouellette, M. I. Saidaminov, G. Walters, A. L. Abdelhady, O. M. Bakr, E. H. Sargent, *Adv. Mater.* **2016**, *28*, 7264.
[4] N. S. Makarov, S. Guo, O. Isaienko, W. Liu, I. Robel, V. I. Klimov, *Nano Lett.* **2016**, *16*, 2349.
[5] J. Pan, S. P. Sarmah, B. Murali, I. Dursun, W. Peng, M. R. Parida, J. Liu, L. Sinatra, N. Alyami, C. Zhao, E. Alarousu, T. K. Ng, B. S. Ooi, O. M. Bakr, O. F. Mohammed, *J. Phys. Chem. Lett.* **2015**, *6*, 5027.
[6] Y. Wang, X. Li, J. Song, L. Xiao, H. Zeng, H. Sun, *Adv. Mater.* **2015**, *27*, 7101.
[7] K. Wu, G. Liang, Q. Shang, Y. Ren, D. Kong, T. Lian, *J. Am. Chem. Soc.* **2015**, *137*, 12792.
[8] K. Nomura, H. Ohta, K. Ueda, T. Kamiya, M. Hirano, H. Hosono, *Science* **2003**, *300*, 1269.
[9] J. F. Wager, *Science* **2003**, *300*, 1245.
[10] Z. Xu, B. M. Sadler, *IEEE Commun. Mag.* **2008**, *46*, 67.
[11] D. Caputo, G. de Cesare, F. Irrera, F. Palma, *IEEE Trans. Electron Devices* **1996**, *43*, 1351.
[12] X. Sheng, C. Yu, V. Malyarchuk, Y.-H. Lee, S. Kim, T. Kim, L. Shen, C. Horng, J. Lutz, N. C. Giebink, J. Park, J. A. Rogers, *Adv. Opt. Mater.* **2014**, *2*, 314.
[13] B. G. Wybourne, *Spectroscopic Properties of Rare Earths*, Interscience Publishers, New York **1965**.
[14] S. Gai, C. Li, P. Yang, J. Lin, *Chem. Rev.* **2014**, *114*, 2343.
[15] H. Lian, Z. Hou, M. Shang, D. Geng, Y. Zhang, J. Lin, *Energy* **2013**, *57*, 270.
[16] N. M. Park, C. J. Choi, T. Y. Seong, S. J. Park, *Phys. Rev. Lett.* **2001**, *86*, 1355.
[17] B. S. Richards, *Sol. Energy Mater. Sol. Cells* **2006**, *90*, 1189.
[18] W. G. J. H. M. van Sark, A. Meijerink, R. E. I. Schropp, J. A. M. van Roosmalen, E. H. Lysen, *Sol. Energy Mater Sol. Cells* **2005**, *87*, 395.
[19] J. H. Warner, A. Hoshino, K. Yamamoto, R. D. Tilley, *Angew. Chem.* **2005**, *117*, 4626.
[20] S. Misra, L. Yu, M. Foldyna, P. Roca i Cabarrocas, *Sol. Energy Mater. Sol. Cells* **2013**, *118*, 90.
[21] S. Qian, S. Misra, J. Lu, Z. Yu, L. Yu, J. Xu, J. Wang, L. Xu, Y. Shi, K. Chen, P. Roca i Cabarrocas, *Appl. Phys. Lett.* **2015**, *107*, 043902.
[22] L. Yu, S. Misra, J. Wang, S. Qian, M. Foldyna, J. Xu, Y. Shi, E. Johnson, P. R. Cabarrocas, *Sci. Rep.* **2014**, *4*, 4357.

[23] F. Priolo, T. Gregorkiewicz, M. Galli, T. F. Krauss, *Nat. Nanotechnol.* **2014**, *9*, 19.
[24] L. Protesescu, S. Yakunin, M. I. Bodnarchuk, F. Krieg, R. Caputo, C. H. Hendon, R. X. Yang, A. Walsh, M. V. Kovalenko, *Nano Lett.* **2015**, *15*, 3692.
[25] G. Nedelcu, L. Protesescu, S. Yakunin, M. I. Bodnarchuk, M. J. Grotevent, M. V. Kovalenko, *Nano Lett.* **2015**, *15*, 5635.
[26] P. Ramasamy, D. H. Lim, B. Kim, S. H. Lee, M. S. Lee, J. S. Lee, *Chem. Commun.* **2016**, *52*, 2067.
[27] J. Lu, S. Qian, Z. Yu, S. Misra, L. Yu, J. Xu, Y. Shi, I. C. P. Roca, K. Chen, *Opt. Express* **2015**, *23*, A1288.
[28] S. Misra, L. Yu, W. Chen, P. Roca i Cabarrocas, *J. Phys. Chem. C* **2013**, *117*, 17786.
[29] L. Yu, F. Fortuna, B. O'Donnell, T. Jeon, M. Foldyna, G. Picardi, P. Roca i Cabarrocas, *Nano Lett.* **2012**, *12*, 4153.
[30] L. Yu, S. Misra, J. Wang, S. Qian, M. Foldyna, J. Xu, Y. Shi, E. Johnson, P. Roca i Cabarrocas, *Sci. Rep.* **2014**, *4*, 4357.
[31] J. Lu, S. Qian, Z. Yu, S. Misra, L. Yu, J. Xu, Y. Shi, P. Roca i Cabarrocas, K. Chen, *Opt. Express* **2015**, *23*, A1288.
[32] R. A. Street, P. Qi, R. Lujan, W. S. Wong, *Appl. Phys. Lett.* **2008**, *93*, 163109.
[33] R. A. Street, W. S. Wong, C. Paulson, *Nano Lett.* **2009**, *9*, 3494.
[34] Y. Zhang, Y. Yu, L. Mi, H. Wang, Z. Zhu, Q. Wu, Y. Zhang, Y. Jiang, *Small* **2016**, *12*, 1062.
[35] Y. Jin, J. Wang, B. Sun, J. C. Blakesley, N. C. Greenham, *Nano Lett.* **2008**, *8*, 1649.
[36] M. Krause, M. Topič, H. Stiebig, H. Wagner, *Phys. Status Solidi (a)* **2001**, *185*, 121.
[37] D. Li, X. Sun, H. Song, Z. Li, Y. Chen, H. Jiang, G. Miao, *Adv. Mater.* **2012**, *24*, 845.
[38] M. Liao, Y. Koide, J. Alvarez, *Appl. Phys. Lett.* **2006**, *88*, 033504.
[39] T. Lin, X. Liu, B. Zhou, Z. Zhan, A. N. Cartwright, M. T. Swihart, *Adv. Funct. Mater.* **2014**, *24*, 6016.
[40] J. Lu, C. Xu, J. Dai, J. Li, Y. Wang, Y. Lin, P. Li, *Nanoscale* **2015**, *7*, 3396.
[41] J. Wang, C. Yan, M.-F. Lin, K. Tsukagoshi, P. S. Lee, *J. Mater. Chem. C* **2015**, *3*, 596.
[42] X. Wang, Y. Zhang, X. Chen, M. He, C. Liu, Y. Yin, X. Zou, S. Li, *Nanoscale* **2014**, *6*, 12009.
[43] R. Hughes, T. Zipperian, L. Dawson, R. Biefeld, R. Walko, M. Dvorack, *J. Appl. Phys.* **1991**, *69*, 6500.